Environmental Science & Technology Letters

Letter

pubs.acs.org/journal/estlcu

Calcium Carbonate Mineralization in a Confined Geometry

Gábor Schuszter, Fabian Brau, and A. De Wit*

Université libre de Bruxelles (ULB), Nonlinear Physical Chemistry Unit, CP231, 1050 Brussels, Belgium

Supporting Information

ABSTRACT: Injection of CO_2 in porous aquifers, where mineralization takes place via chemical reactions, is one possible long-term solution considered for storage of this greenhouse gas. This mineralization is investigated here experimentally in a confined geometry by injecting radially an aqueous solution of carbonate into a solution of calcium ions to produce solid calcium carbonate. Various precipitation patterns are observed depending on the injection rate and concentrations of the reactants. The pattern properties are quantified to analyze the influence of the growth conditions on mineralization. We show the existence of critical concentrations of reactants, which are functions of the flow rate, above which the amount of precipitate drops significantly.

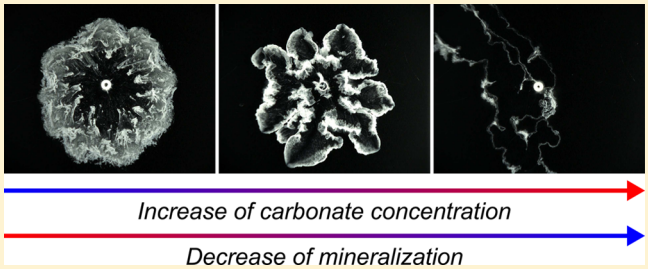

INTRODUCTION

To reduce atmospheric concentrations of CO_2, a possible solution is its sequestration in depleted oil[1] or gas reservoirs, or in saline aquifers.[2] In such aquifers, transport and reactive processes take place during the CO_2 plume migration, such as wormholing[3] and precipitation.[4,5] Mineral carbonation is particularly interesting because it offers safe long-term storage of CO_2. In this mineralization, carbonates resulting from dissolution of CO_2 in water react with mineral ions (such as Ca^{2+} or Mg^{2+}) to produce harmless solid precipitates trapped in the soils.

Such a precipitation at the miscible interface between two reactive solutions can lead to fingering in porous media due to a local decrease in permeability.[6] It is of interest to understand how such fingering can affect the efficiency of CO_2 mineralization in terms of the amount of solid phase produced and of its spatial distribution. However, insight into such problematics is difficult to assess *in situ*.

In this context, we study here experimentally precipitation patterns of calcium carbonate ($CaCO_3$) by radial injection in a horizontal confined reactor[7−10] of a solution of carbonates (CO_3^{2-}) into a solution of calcium ions (Ca^{2+}). This mimics the situation in which carbonates resulting from dissolution of CO_2 in water react with mineral ions present in that water. The precipitate is produced by the reaction $Ca_{(aq)}^{2+} + CO_{3(aq)}^{2-} \rightleftharpoons CaCO_{3(s)}$. A large variety of patterns is obtained when the reactant concentrations and flow rate are varied. We characterize quantitatively the area of the pattern covered by the precipitate, its radial extent, and its spatial distribution. We find that the amount of precipitate varies with the injection speed and the concentration of reactants, the smallest amount being produced at high values of these parameters.

MATERIALS AND METHODS

Experiments are performed in a horizontal Hele-Shaw cell consisting of two parallel transparent Plexiglas plates (19.5 cm × 19.5 cm) separated by a small interstice (0.5 mm). The cell is illuminated from above by two light pads placed symmetrically with respect to a digital camera recording the dynamics. The cell is initially filled by an aqueous solution of $CaCl_2$. An aqueous solution of Na_2CO_3 is injected radially from the center of the lower plate through an inlet with a 1 mm inner diameter using a syringe pump. The pH of this solution is adjusted to 10 by addition of 2 mol/L HCl to avoid the production of solid calcium hydroxide $Ca(OH)_2$. The injection is performed at a constant flow rate Q in the range of those used for displacements in well-bore samples.[4] The two other control parameters are the normalized concentrations of reactants, $[X]_n = c_x/c_{max}$, which are their dimensional concentrations (c_x) divided by their solubility in water, c_{max}, at (21 ± 1) °C (Table S1 of the Supporting Information).

Panels a−c of Figure 1 show a representative time sequence of the precipitation dynamics. At the beginning of radial injection, the contact zone between the two solutions grows as an expanding circle (Figure 1a). The formation of the precipitate decreases locally the mobility of the reactive zone displaced by the injected solution of higher mobility. This unstable situation[6] leads to the emergence of fingers (Figure 1b). Depending on the contrast in mobility, the amplitude of this destabilization may be small, leading to almost circular patterns or large with pronounced fingers and a nonuniform spatial distribution.

Received: January 26, 2016
Revised: March 26, 2016
Accepted: March 28, 2016
Published: March 28, 2016

DOI: 10.1021/acs.estlett.6b00074
Environ. Sci. Technol. Lett. 2016, 3, 156−159

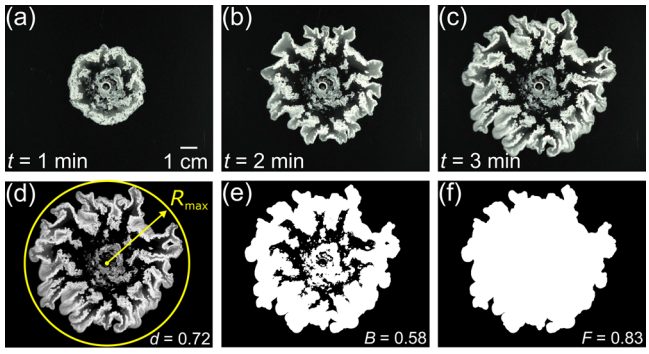

Figure 1. (a–c) Time evolution of a fingered precipitation pattern. (d–f) Variables used to characterize the patterns. (d) Distribution of grayscale intensity $I(x,y)$. The yellow circle passing by the tip of the longest finger defines the radius R_{max}. (e) Area A covered by the solid phase. (f) Area A_p inside the pattern perimeter.

To study the effect of initial reactant concentrations and flow rate on precipitate pattern formation, a quantitative image analysis is performed. We measure the grayscale value, $I(x,y,t)$, of the images of the dynamics where x and y are spatial coordinates. We compute a normalized intensity $I_n \in [0,1]$ as $I_n(x,y) = [I(x,y) - I_{back}(x,y)]/(I_{max} - I_{min})$, where $I_{back}(x,y)$ is the grayscale intensity of a background image (taken before the experiment starts) and I_{max} and I_{min} are its maximal and minimal values, respectively. Finally, $I_n(x,y)$ is set to 0 if it is smaller than some threshold $I_{th} = 0.05$. This threshold fixes the smallest intensity below which we cannot determine with certainty the presence of a precipitate. An example of the spatial distribution of $I_n(x,y,t)$ is shown in Figure 1d. Radius R_{max} is the largest radial distance between the injection point and the pattern perimeter. For each image, we also compute (i) area A covered by the pattern (Figure 1e), i.e., the area where $I_n > I_{th}$, and (ii) area A_p of the zone inside the pattern perimeter (Figure 1f).

We next define four quantities to measure the pattern properties. The first quantity is the total grayscale intensity, $I_{tot}(t) = \int I_n(x,y,t)\, dx\, dy \in [0,A]$, where $0 < A < N = 1280 \times 1024$ pixels of the image resolution. Even though a given I_{tot} might correspond to various precipitate thicknesses within the cell, it qualitatively indicates the amount of precipitate in the gap because of its white color. The second quantity is the brightness of the precipitate, $B = I_{tot}/A$, normalizing its total grayscale intensity I_{tot} by the area A it is covering (Figure 1e). B varies between 0 and 1, with values close to 1 indicating a concentrated bright precipitate. The third quantity is the filling of the pattern, $F = A/A_p \in [0,1]$, dividing its area A by the area A_p enclosed by its perimeter (Figure 1f). F is less than 1 if the pattern contains some black areas without precipitate. A case for which $F \ll 1$ indicates a hollow mineralization structure. The last quantity is the pattern density, $d = A_p/(\pi R_{max}^2) \in [0,1]$, comparing the area A_p of the pattern to the area of the circle of radius R_{max} (Figure 1d).[10] It measures deviations from a symmetric radial growth (for which $d = 1$). Low values of d indicate that precipitation occurs in some preferred directions.

RESULTS AND DISCUSSION

Figure 2 shows the various patterns obtained under different experimental conditions after injecting 3 mL of a CO_3^{2-} solution into the Ca^{2+} solution. Considering the concentrations (Table S1 of the Supporting Information) and the activity coefficients for the related solutions,[11,12] the saturation index SI = $\log_{10}(IAP/K_{SP})$ can be calculated as being in the range of

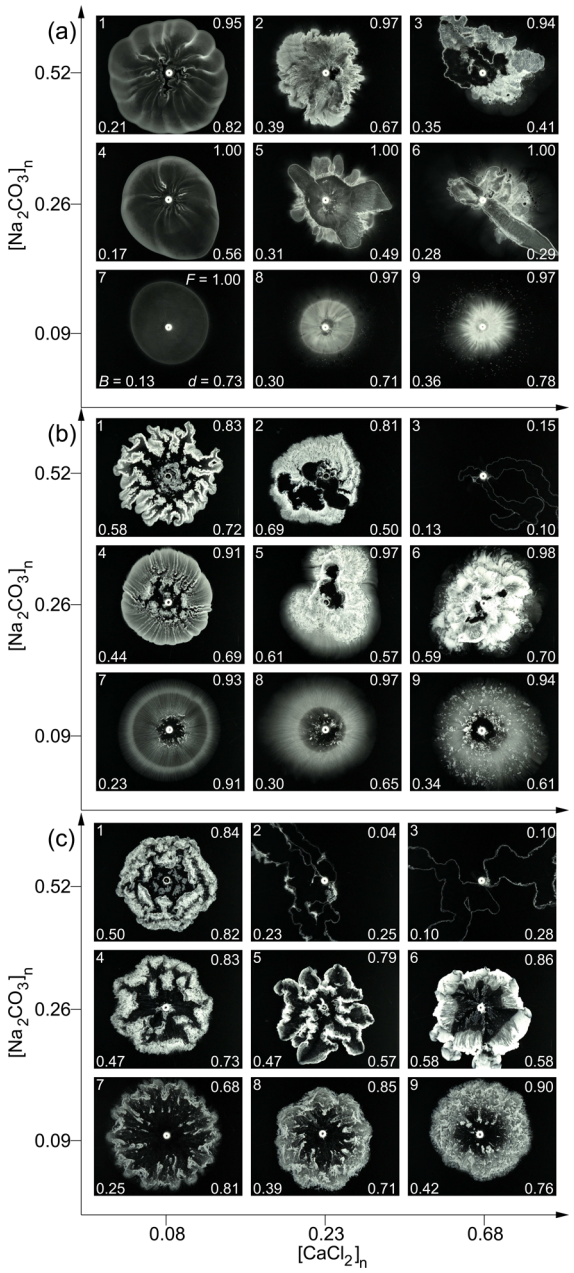

Figure 2. Patterns observed at different flow rates and concentrations (122 mm × 98 mm field of view). The numbers at the top left, bottom left, top right, and bottom right corners are the pattern number, B, F, and d, respectively (see pattern a7). (a) $Q = 0.1$ mL/min ($t = 30$ min). (b) $Q = 1.0$ mL/min ($t = 3$ min). (c) $Q = 6.5$ mL/min ($t = 28$ s).

6.8–9.1 (Table S2 of the Supporting Information). Here IAP and K_{SP} are the ion activity product of the reactant mixture and the solubility product of $CaCO_3$, respectively. The high SI values show that the reactant mixture is highly supersaturated in the localized reaction zone at the interface between the carbonate and calcium solutions. Precipitation occurs thus fast, and the Damköhler number (ratio of hydrodynamic to chemical time scales) is expected to be large in each case.

Let us first examine the patterns obtained for various flow rates at the lowest concentrations for both reactants. At the lowest flow rate (Figure 2a7), a circular structure grows homogeneously. The amount of precipitate is small, which gives a low brightness $B = 0.13$. The $F = 1$ value indicates that some

DOI: 10.1021/acs.estlett.6b00074
Environ. Sci. Technol. Lett. 2016, 3, 156–159

precipitate is produced everywhere within the pattern perimeter as for all patterns at the lowest flow rate. Small radial stripes appear at the periphery when Q is increased (Figure 2b7 and Movie S1). They originate from buoyancy-driven convection due to a density gradient.[13] The radial symmetry is, however, preserved, but the precipitate starts to be flushed away from the injection point by the flow; F is thus slightly smaller than 1. Increasing further the flow rate destabilizes the pattern perimeter in fingers, which breaks the radial symmetry (Figure 2c7). The enhanced flow advects the precipitate to the periphery of the structure, leading to a smaller value of F. In some cases, spirals can be observed (Figure 2c5 and Movie S2) similar to those studied for other chemicals.[8]

Keeping the concentration of one of the reactants at its lowest value and increasing the concentration of the other reactant lead to a larger amount of precipitate and hence to an increase in I_{tot} and B. The effect on I_{tot} is more pronounced when the concentration of carbonate is increased at a fixed calcium concentration than in the reverse case (Figure 3). This

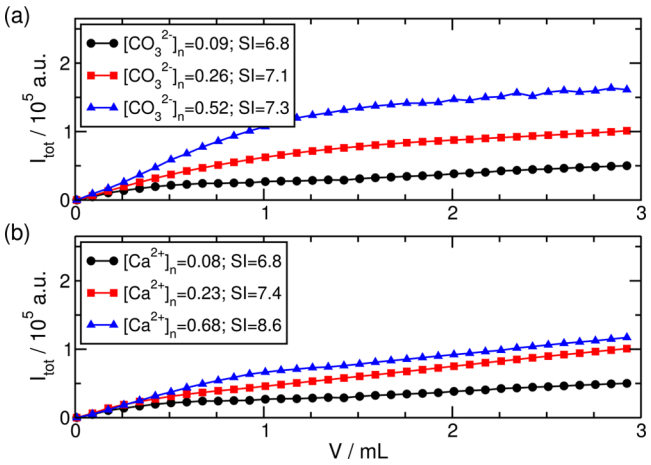

Figure 3. Evolution of I_{tot} as a function of injected volume V of a carbonate solution at Q = 0.1 mL/min. (a) $[Ca^{2+}]_n$ = 0.08, and $[CO_3^{2-}]_n$ varies. (b) $[CO_3^{2-}]_n$ = 0.09, and $[Ca^{2+}]_n$ varies.

could be explained by the relatively larger change in viscosity of the Ca^{2+} solution (see Table S1) as the concentration increases, which hinders the mixing of the reactants when the less viscous CO_3^{2-} is injected. The influence of various mixing effects due to the flow[7,14] on underlying reaction−diffusion profiles[6] should also be investigated to improve our understanding of these differences.

The evolution of I_{tot} as a function of flow rate is shown in Figure 4a,b. One might intuitively expect that the regime where most precipitate is produced is reached when the concentrations of both reactants are high. This is, however, not the case. At a large enough constant flow rate Q, increasing the concentration of both reactants leads to patterns showing barely any precipitate (Figure 2b3 and Figure 2c2,3) even though the SI is high in the reaction zone. These patterns take the form of wide hollow tubes because the injected carbonate solution channels through the calcium one without much mixing and precipitation. Similarly, at sufficiently large given concentrations of both reactants, increasing the flow rate Q leads to a strong decrease in the B value and I_{tot} (Figure 4c), indicating a sharp drop in the level of mineralization.

To understand the evolution of these hollow patterns, note that the ratio between the viscosity of the displaced Ca^{2+} and

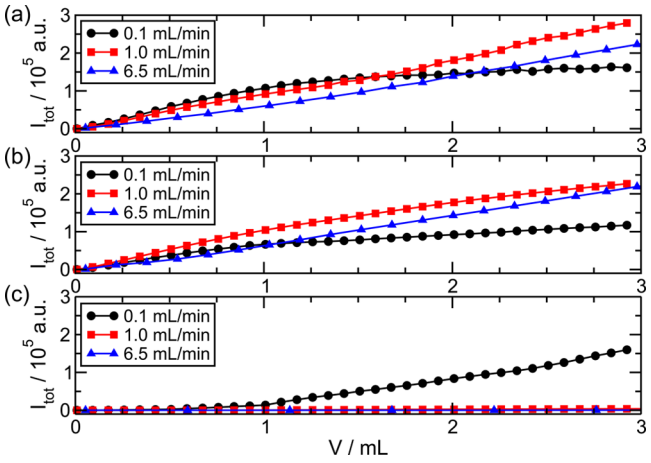

Figure 4. Evolution of I_{tot} as a function of injected volume V for different flow rates. (a) $[Ca^{2+}]_n$ = 0.08, $[CO_3^{2-}]_n$ = 0.52, and SI = 7.3. (b) $[Ca^{2+}]_n$ = 0.68, $[CO_3^{2-}]_n$ = 0.09, and SI = 8.6. (c) $[Ca^{2+}]_n$ = 0.68, $[CO_3^{2-}]_n$ = 0.52, and SI = 9.1.

that of the injected CO_3^{2-} solution is only ∼3 (Table S1). As shown previously,[10] this viscosity contrast is not large enough to produce viscous fingering under our experimental conditions. However, as soon as the reactants are in contact, precipitation occurs along the flow, producing a cohesive precipitate barrier between the two reactants with a random shape (Figure 2b3 and Figure 2c2,3). New precipitate layers next form along the fast-moving liquid−liquid interface, giving precipitate walls that thicken and become more rigid (Movie S3). The stiffness of these walls allows the interior pressure to be sustained, inhibiting further mixing of the reactant solutions. Then, the barrier thickens only slowly from secondary reaction−diffusion growth on a much longer time scale (hours compared to 28 s of experimental time in the case of Q = 6.5 mL/min). These tubelike patterns are characterized by low d values due to an asymmetric geometry.

The various trends observed in Figure 2 can be summarized as follows. (i) Homogeneous circular patterns are obtained at low concentrations and low flow rates Q. In that case, brightness B is small and filling F is close to 1, which indicates that there is a small amount of precipitate everywhere inside the perimeter with a pattern density d close to 1. When flow rate Q increases, some fingering appears and F decreases. (ii) If the concentration of one of the two reactants is kept low and the other is increased, more precipitate is formed with an increase in B. Heterogeneities in the distribution of the precipitate appear at large Q values. (iii) For high concentrations of both reactants and beyond some Q, we observe hollow tubes with a sharp drop in the production of precipitate even if the SI remains high, and asymmetries in the distribution leading to low values of B, F, and d.

The implications for CO_2 storage are as follows. For low concentrations of minerals (i.e., Ca^{2+} here) in the soil, the amount of precipitate increases with the concentration of carbonate (related to the amount of CO_2 injected) as shown in Figure 3a, with a slight influence of Q (Figure 4a). For higher concentrations of minerals, the amount of precipitate first increases with the concentration of carbonate before sharply dropping down beyond some critical value $[Ca^{2+}]_n^c$, which decreases as Q increases (see Figures 2 and 4). At the lowest flow rate (Q = 0.1 mL/min), this critical concentration $[Ca^{2+}]_n^c$ has not been reached here. At Q = 1 mL/min, we find that 0.23

DOI: 10.1021/acs.estlett.6b00074
Environ. Sci. Technol. Lett. 2016, 3, 156−159

< $[Ca^{2+}]_n^c$ < 0.68, and at Q = 6.25 mL/min, 0.08 < $[Ca^{2+}]_n^c$ < 0.23.

Pattern formation during $CaCO_3$ mineralization has been studied experimentally during radial injection of an aqueous solution of carbonate into a solution of Ca^{2+} within a confined geometry. The amount of precipitate, as well as its spatial distribution, depends on the concentrations of the reactants and on Q. The patterns have been characterized by their grayscale intensity, spatial area, and perimeter to quantify the amount of minerals produced and the geometry of the pattern. We find that, above critical values of concentrations that depend on flow rate Q, the amount of precipitate drops significantly even if the SI in the localized reaction zone is large. This suggests that the highest efficiency of $CaCO_3$ mineralization is not obtained necessarily at high concentrations and high Q values. Our analysis paves the way to numerous possible experimental and theoretical extensions. From a theoretical point of view, the effect of flow and mixing on precipitation should be further analyzed to understand the conditions under which precipitation drops even if the SI remains large, as observed here. The robustness of our conclusions could be tested experimentally with changes in the reactants, viscosity, pressure, temperature, and pH, both in simple Hele-Shaw cells and in more complex geometries, including Hele-Shaw cells with obstacles or beads to vary the porosity and real three-dimensional porous systems.

■ ASSOCIATED CONTENT

Supporting Information

The Supporting Information is available free of charge on the ACS Publications website at DOI: 10.1021/acs.estlett.6b00074.

Description of solution properties (Table S1) and the saturation index for reactant concentration pairs (Table S2) (PDF)

Temporal evolution of pattern 7 shown in Figure 2b (accelerated 10 times, Movie S1) (AVI)

Temporal evolution of pattern 5 shown in Figure 2c (accelerated 4 times, Movie S2) (AVI)

Temporal evolution of pattern 3 shown in Figure 2c (accelerated 15 times, Movie S3) (AVI)

■ AUTHOR INFORMATION

Corresponding Author

*E-mail: adewit@ulb.ac.be. Phone: +32 2 650 5774. Fax: +32 2 650 5767.

Notes

The authors declare no competing financial interest.

■ ACKNOWLEDGMENTS

We thank Prodex for financial support.

■ REFERENCES

(1) Dai, Z.; Middleton, R.; Viswanathan, H.; Fessenden-Rahn, J.; Bauman, J.; Pawar, R.; Lee, S.-Y.; McPherson, B. An Integrated Framework for Optimizing CO_2 Sequestration and Enhanced Oil Recovery. *Environ. Sci. Technol. Lett.* **2014**, *1*, 49−54.

(2) Metz, B., Davidson, O., de Coninck, H. C., Loos, M., Meyer, L. A., Eds. *IPCC Special Report on Carbon Dioxide Capture and Storage*; Cambridge University Press: New York, 2005.

(3) Chadam, D.; Hoff, D.; Merino, E.; Ortoleva, P.; Sen, A. Reactive Infiltration Instabilities. *J. Appl. Math.* **1986**, *36*, 207−221.

(4) Luquot, L.; Gouze, P. Experimental Determination of Porosity and Permeability Changes Induced by Injection of CO_2 into Carbonate Rocks. *Chem. Geol.* **2009**, *265*, 148−159.

(5) White, A. R.; Ward, T. CO_2 Sequestration in a Radial Hele-Shaw Cell via an Interfacial Chemical Reaction. *Chaos* **2012**, *22*, 037114.

(6) Nagatsu, Y.; Ishii, Y.; Tada, Y.; De Wit, A. Hydrodynamic Fingering Instability Induced by a Precipitation Reaction. *Phys. Rev. Lett.* **2014**, *113*, 024502.

(7) Tartakovsky, A. M.; Redden, G.; Lichtner, P. C.; Scheibe, T. D.; Meakin, P. Mixing-Induced Precipitation: Experimental Study and Multiscale Numerical Analysis. *Water Resour. Res.* **2008**, *44*, W06S04.

(8) Haudin, F.; Cartwright, J. H. E.; Brau, F.; De Wit, A. Spiral Precipitation Patterns in Confined Chemical Gardens. *Proc. Natl. Acad. Sci. U. S. A.* **2014**, *111*, 17363−17367.

(9) Zhang, C.; Dehoff, K.; Hess, N.; Oostrom, M.; Wietsma, T. W.; Valocchi, A. J.; Fouke, B. W.; Werth, J. C. Pore-Scale Study of Transverse Mixing Induced $CaCO_3$ Precipitation and Permeability Reduction in a Model Subsurface Sedimentary System. *Environ. Sci. Technol.* **2010**, *44*, 7833−7838.

(10) Haudin, F.; De Wit, A. Patterns Due to an Interplay Between Viscous and Precipitation-Driven Fingering. *Phys. Fluids* **2015**, *27*, 113101.

(11) Staples, B. R.; Nuttall, R. L. The Activity and Osmotic Coefficients of Aqueous Calcium Chloride at 298.15 K. *J. Phys. Chem. Ref. Data* **1977**, *6*, 385−407.

(12) Robinson, R. A.; Macaskill, J. B. Osmotic Coefficients of Aqueous Sodium Carbonate Solutions at 25°C. *J. Solution Chem.* **1979**, *8*, 35−40.

(13) Haudin, F.; Riolfo, L. A.; Knaepen, B.; Homsy, G. M.; De Wit, A. Experimental Study of a Buoyancy-Driven Instability of a Miscible Horizontal Displacement in a Hele-Shaw Cell. *Phys. Fluids* **2014**, *26*, 044102.

(14) De Simoni, M.; Carrera, J.; Sánchez-Vila, X.; Guadagnini, A. A Procedure for the Solution of Multicomponent Reactive Transport Problems. *Water Resour. Res.* **2005**, *41*, W11410.

DOI: 10.1021/acs.estlett.6b00074
Environ. Sci. Technol. Lett. 2016, 3, 156−159